ACS APPLIED POLYMER MATERIALS

pubs.acs.org/acsapm Article

Comparison of Bulk- vs Layer-by-Layer-Cured Stimuli-Responsive PNIPAM−Alginate Hydrogel Dynamic Viscoelastic Property Response via Embedded Sensors

Yang Liu, Keturah Bethel, Manjot Singh, Junru Zhang, Rana Ashkar, Eric M. Davis, and Blake N. Johnson*

Cite This: ACS Appl. Polym. Mater. 2022, 4, 5596−5607 Read Online

ACCESS | Metrics & More | Article Recommendations | Supporting Information

ABSTRACT: While stimuli-responsive hydrogels are now being widely investigated, such as for additive manufacturing applications, it remains a challenge to continuously monitor the dynamic response of their material properties to stimuli using traditional characterization methods. Here, we report that dynamic-mode piezoelectric milli-cantilever sensors enable real-time monitoring of the viscoelastic response of bulk- and layer-by-layer (LBL)-cured composite poly(*N*-isopropylacrylamide) (PNIPAM)−alginate hydrogel constructs to thermal changes across the 25−37 °C temperature range. Scanning electron microscopy and sensing studies revealed that the network structure and viscoelastic response of ionic−covalent entanglement composite PNIPAM−alginate hydrogel constructs are dependent on the hydrogel processing method. Composite PNIPAM−alginate constructs fabricated using LBL curing exhibited relatively increased responsiveness compared to bulk-cured constructs in terms of the magnitude of thermal stimulus-driven shear storage modulus change, suggesting opportunities for additive manufacturing applications. In summary, we show that sensors, in combination with traditional characterization methods, enable the study of dynamic process−structure−rheological property relations of stimuli-responsive soft materials and real-time monitoring of material rheological properties using a low-sample volume measurement format.

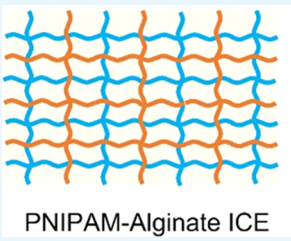

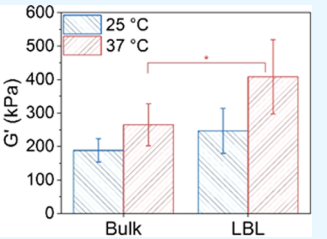

KEYWORDS: *stimuli-responsive hydrogel, composite hydrogel, monitoring, sensing, cantilever*

1. INTRODUCTION

Additive manufacturing using stimuli-responsive hydrogels has enabled emerging applications that require dynamic property or shape change, including soft robotics and shape memory actuators.[1−3] Hydrogels are viscoelastic materials composed of a three-dimensional (3D) polymer network that contain high amounts of water.[4] Stimuli-responsive hydrogels exhibit temporal changes in structure, properties, and shape in response to environmental stimuli.[5−8] Various stimuli have been examined for actuation of hydrogel response, including physical (e.g., temperature, electric field, magnetic field, light), chemical (e.g., pH), and biological stimuli (e.g., affinity ligands, enzyme substrates). For example, poly(*N*-isopropylacrylamide) (PNIPAM)−water mixtures, which exhibit a lower critical solution temperature (LCST) of 32 °C, are widely investigated thermo-responsive hydrogels.[9] In addition to hydrogels composed of a single polymer component, composite hydrogels have also received considerable attention based on their unique properties that may arise from interactions among different polymer species. Understanding of process−structure−property relations of composite hydrogels remains an active area of research. Composite hydrogels have been already utilized in a range of smart applications. Bakarich et al. fabricated a smart valve of PNIPAM−alginate hydrogels using microextrusion printing to control water flow rate.[10] The valve closed and opened upon exposure to hot and cold water, respectively, based on the thermal expansion of the hydrogel over the 20−60 °C temperature range. To date, various additive manufacturing processes have utilized PNIPAM and composite PNIPAM hydrogels to fabricate layer-by-layer (LBL) constructs in various geometries, such as dumbbell-shaped structures, flower biomimetics, tubes, and so on.[11−15] However, there remains a need to investigate potential process−material interactions that may affect the quality of layered hydrogel constructs (i.e., fabricated by LBL curing-based processing methods, such as additive manufacturing processes) in terms of resultant properties and stimuli response. In particular, new methods for real-time monitoring

Received: April 13, 2022
Accepted: July 6, 2022
Published: July 18, 2022

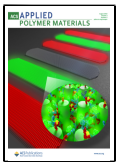

https://doi.org/10.1021/acsapm.2c00634
ACS Appl. Polym. Mater. 2022, 4, 5596−5607

of material dynamic response to stimuli could yield new insights into the design of stimuli-responsive hydrogels.

While a variety of methods have been established to characterize the structure and properties of hydrogels, relatively few are able to assess the real-time response of stimuli-responsive hydrogels. For example, while compressive testing is commonly utilized for characterization of hydrogel modulus, the method involves relatively long manual sample preparation and testing times.[16−18] In addition to mechanical properties, the passive swelling response of hydrogels in water based on weight or volume change measurements provides a common method of characterizing hydrogel microstructure, including the density of crosslinking, average molecular weight between crosslinks, and mesh size.[19−21] Scanning electron microscopy (SEM) can also provide insight into the microstructure and morphology of hydrogels based on image data.[22−24] Another method for characterizing hydrogel morphology is small-angle neutron scattering (SANS), which is useful for investigating the phase behavior, such as phase separation of PNIPAM.[25−27] More recently, confocal laser scanning microscopy (CLSM) has been applied to evaluate the structure of complex synthetic materials, including hydrogels.[28] Fluorescently stained hydrogels can be imaged without the need for sample freeze-drying, enabling visualization of the static and dynamic structure via time-lapse CLSM. For instance, Si et al. studied the effect of acrylic acid weight percentage on the pore size in poly(*N*-isopropylacrylamide-*co*-acrylic acid) microspheres, and Kubota et al. imaged the pH-responsive hydrogelation process of a peptide-grafted polymer.[29,30] In addition to characterization of hydrogel mechanical properties based on uniaxial testing, characterization of hydrogel rheological properties is also commonly utilized in hydrogel materials research. For example, hydrogel rheological properties provide insight into gelation processes as well as hydrogel processability. Rheological properties can also provide insight into hydrogel microstructures.[31−33] For instance, Karvinen et al. quantified the average mesh size, crosslinking density, and average molecular weight of the polymer chain between neighboring crosslinks of hydrazone crosslinked polysaccharide hydrogels by applying amplitude and frequency sweep measurements obtained by dynamic mechanical analysis (DMA).[34] Despite these advances, the ability to characterize the real-time response of hydrogel structure and properties in response to stimuli is still a bottleneck, especially using measurement formats that involve minimal sample preparation and small sample volumes.

Unlike the majority of traditional characterization methods, which are constrained by low throughput and time-to-results due to intensive manual sample preparation and lengthy characterization tests, sensor-based material characterization methods exhibit various advantages, including transducers that exhibit high sensitivity, continuous monitoring, reduction of required sample size and preparation time, and potentially improved reproducibility relative to methods that involve intensive manual sample preparation.[35−37] Quartz crystal microbalance with dissipation monitoring (QCM-D) technology, for example, has been effectively used to characterize the viscoelastic response and properties of PNIPAM hydrogel thin films. Changes in temperature-driven frequency and dissipation factor enabled monitoring of viscoelasticity and structure response of PNIPAM hydrogels during phase transition.[38] However, QCM-D is typically limited to characterization of thin-film structures. In addition, QCM sensors may exhibit form factors that are challenging to scale and integrate within practical material processes (e.g., additive manufacturing processes) for purposes of online process monitoring and control. High-speed atomic force microscopy performed by Matsui et al. was reported to detect the size and morphology change of PNIPAM at the individual microgel level.[39] Haring et al. showed that dynamic-mode piezoelectric milli-cantilever (PEMC) sensors enabled characterization of gelatin and alginate hydrogel viscoelastic properties and continuous monitoring of sol−gel phase transitions.[35] Cesewski et al. further showed that high-order modes of PEMC sensors near 800 kHz enable sensitive characterization of hydrogel viscoelastic properties.[36] Using cantilever sensors for real-time monitoring, Singh et al. designed a closed loop to control the photopolymerization process for the fabrication of photocurable hydrogels with controlled storage moduli.[37] Thus, it is of interest to examine the potential for PEMC sensors to characterize the real-time stimuli response of bulk-cured vs layered PNIPAM-based hydrogels

Here, we show that dynamic-mode PEMC sensors facilitate real-time monitoring of multistep composite ionic−covalent entanglement (ICE) PNIPAM−alginate hydrogel gelation processes and composite hydrogel response to temperature change. We further compare the difference in the network structure and viscoelastic properties of composite hydrogels fabricated by bulk- vs LBL-curing processes. Hydrogel viscoelastic properties obtained by sensor data and cantilever fluid−structure interaction were benchmarked against DMA.

2. MATERIALS AND METHODS

2.1. Materials. Alginic acid sodium salt (AlgNa), 2,2-dimethoxy-2-phenylacetophenone (DMPA), calcium chloride ($CaCl_2$), *N*-isopropylacrylamide (NIPAM), and *N*,*N*′-methylenebisacrylamide (MBAA) were purchased from Sigma-Aldrich. Lead zirconate titanate (PZT-5A, 72.4 × 72.4 × 0.127 mm^3) with nickel (Ni) electrodes was from Piezo Systems (Woburn, MA). Glass cylinders and ethanol (200 proof) were from Fisher Scientific. Polyurethane (Fast-Drying) and epoxy (EA 1C-LV) were from Minwax and Loctite, respectively.

2.2. Fabrication of Piezoelectric-Excited Millimeter Cantilever Sensors. PEMC sensors (n = 5) were fabricated from Ni-electroded lead zirconate titanate (PZT) as described in our other studies.[35,36,40] Briefly, PZT sheets were diced into chips (5 × 1 × 0.127 mm^3; American Dicing, Liverpool, NY). Insulated wires (30-gauge; copper) were soldered to the top and bottom faces of the Ni electrodes on the distal end of the PZT layer. The soldered distal end of the chip, including solder points, was then potted in a glass cylinder (6 mm diameter) with a nonconductive epoxy, resulting in a cantilever geometry (3 × 1 × 0.127 mm^3). Additional epoxy was applied on one side of the PZT to create an asymmetric anchor.[40] The sensors were subsequently coated with polyurethane via brush coating and allowed to cure at room temperature. Following polyurethane coating, the sensors were then coated with parylene C (∼10 μm thick) following vendor protocols (PDS 2010 Labcoter 2, Specialty Coating Systems; Indianapolis, IN). Following parylene C coating, the sensors were annealed for 1 h at 75 °C.

2.3. Real-Time Sensor-Based Monitoring of Hydrogel Gelation and Thermal Response. The precursor solution for the composite ICE PNIPAM−alginate hydrogel was prepared by vigorously mixing alginate stock solution (2 wt % of AlgNa/water), NIPAM, MBAA, DMPA stock solution (1 wt % of DMPA/ethanol), and deionized water. The concentration of alginate and NIPAM in the final solution were 1 and 8 wt %, respectively. The concentration of DMPA and MBAA in the final solution were 0.15 and 0.5%, respectively, with respect to the NIPAM monomer concentration. The solution used for NIPAM hydrogels exhibited the same formulation but did not contain alginate.

https://doi.org/10.1021/acsapm.2c00634
ACS Appl. Polym. Mater. 2022, 4, 5596−5607

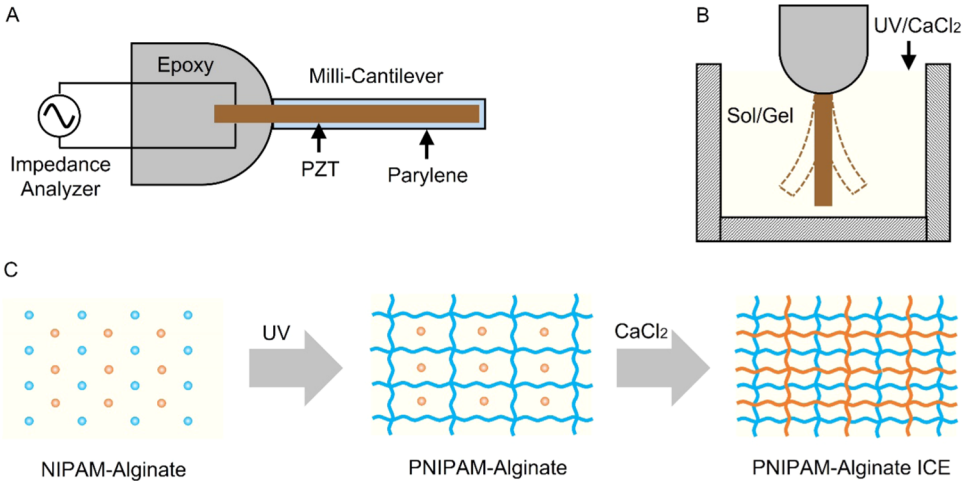

Figure 1. Schematic of a PEMC sensor (A) and measurement format (B) for real-time monitoring of ICE composite PNIPAM−alginate hydrogel assembly, gelation, and viscoelastic property response. (C) Crosslinking process and network structure associated with ICE composite PNIPAM−alginate hydrogels.

Gelation studies were performed in a custom aluminum mold (length × width × height = 39 × 21 × 13 mm^3; see Figure S1). The mold was immersed in a water bath (20 °C) for temperature control. Prior to all experiments, the sensor was positioned 0.2 mm from the bottom of the mold using a manual micromanipulator. The sensor resonant frequency (f) and phase angle at resonance (ϕ) were continuously monitored and acquired with a vector network analyzer with the impedance option (E5061b-005; Keysight) and a custom MATLAB program. The phase angle of the PEMC sensor, which is defined as $\phi = \arctan[\mathrm{Im}(Z)/\mathrm{Re}(Z)]$, where Z is the electrical impedance of the piezoelectric layer of the PEMC sensor, should not be confused with the phase lag associated with the viscoelastic response of the surrounding material. The phase angle of a resistor−capacitor (RC) circuit is between −90 and 0°, since the reactive capacitance (X_C) is often defined as a negative value by convention (i.e., $X_C = -1/(\omega C)$, where ω is the angular frequency and C is the capacitance). Thus, since the phase angle is negative, the current leads the applied voltage in an RC circuit. As discussed, the phase angle of the PEMC sensor is different than the phase lag (δ) between applied stress and resultant strain in the surrounding viscoelastic material that results from the oscillating cantilever, which is defined as $\delta = \arctan[\mathrm{Im}(G^*)/\mathrm{Re}(G^*)] = \arctan[G''/G']$, where $G^* = (G'^2 + G''^2)^{0.5}$ is the complex shear modulus of the surrounding material, here, a polymer solution or hydrogel. While the phase angle of an RC circuit, such as a PEMC sensor, ranges from −90 to 0°, δ ranges from 0 to 90°. While ϕ and δ are different physical quantities, as discussed, the change in ϕ is governed by the motional changes in the circuit resistance, capacitance, and inductance, which are dependent on the surrounding material's viscoelastic properties (and thus, δ). Thus, it is possible to characterize changes in the surrounding material's viscoelastic properties (a mechanical system), by measuring changes in the frequency response of the electrical circuit formed by the PEMC sensor (an electromechanical system) that is mechanically coupled to the sensor through fluid−structure interaction effects.[41] Electrical impedance analysis was performed using a stimulus amplitude of 100 mV alternating current (AC) and zero direct current (DC) bias across a frequency range ($f \pm 10$ kHz).

Following stabilization of the sensor signals, bulk-cured hydrogels were prepared by adding 1 mL of precursor solution to the mold. Bulk-cured composite PNIPAM−alginate hydrogels were prepared by first photocuring NIPAM for 30 min (365 nm; UVGL-58; UVP) to form the PNIPAM network. The alginate network and resultant ICE composite PNIPAM−alginate hydrogel was subsequently formed by ionic crosslinking by depositing a 100 μL droplet of calcium chloride (500 mM) on the surface of the material approximately 5 mm from the submerged sensor. PNIPAM and alginate hydrogels served as the negative controls and were synthesized by the same methods. Four-layer LBL-cured composite PNIPAM−alginate hydrogel constructs were prepared by LBL photocuring (250 μL per layer) over the course of 80 min. Following the photocuring of each layer, the alginate network was ionically crosslinked by depositing a 100 μL droplet of calcium chloride (500 mM) on the surface of the multilayer construct approximately 5 mm from the submerged sensor. For investigation of hydrogel thermal response, the hydrogels were cycled from 25 to 37 to 25 °C.

2.4. Data Analysis. The resonance amplitude, A, (i.e., peak height) was calculated as the difference between the phase angle at resonance (ϕ) and the baseline phase angle off-resonance (ϕ_0). For example, the resonance amplitude of the cantilever sensor in air was given as $A_{Air} = \phi_{Air} - \phi_0$. Thus, A_{Air}, $A_{Solution}$, A_{UV}, and A_{CaCl_2} represented the change in ϕ relative to the baseline value in air associated with the precursor solution, photocured hydrogel, and chemically-crosslinked hydrogel, respectively. To describe the PNIPAM gelation process, the percent change of the resonance amplitude caused by photocuring was calculated by $\Delta A_{UV} = (A_{UV} - A_{Solution})/A_{Solution} \times 100$. Similarly, the percent change of resonance amplitude caused by calcium chloride crosslinking was $\Delta A_{CaCl_2} = (A_{CaCl_2} - A_{Solution})/A_{Solution} \times 100$. The composite PNIPAM−alginate hydrogels required two sequential reactions for preparation. For comparison of composite PNIPAM−alginate and alginate hydrogels, the percent change of the second step ($CaCl_2$ crosslinking) relative to the first step (UV curing) was calculated as $\Delta A_{CaCl_2} = (A_{CaCl_2} - A_{UV})/A_{UV} \times 100\%$. We also define $\Delta A_{UV} = (A_{UV} - A_{Air})/A_{Air} \times 100\%$ when comparing the gelation of bulk- vs LBL-photocured hydrogels, given the absence of $A_{Solution}$ for the reaction. Significance testing was performed using a Student's t-test (Microsoft Excel).

2.5. Characterization of Hydrogel Low-Frequency Viscoelastic Moduli via Dynamic Mechanical Analysis. Characterization of hydrogel low-frequency compressive storage and loss moduli (E' and E'', respectively) was done using a dynamic mechanical analyzer (Q800; TA Instruments). Hydrogel specimens were prepared using a custom mold (diameter = 10 mm; height ∼ 5 mm). All measurements were acquired at 25 °C by application of a 15 μm periodic displacement at a constant frequency (1 Hz) and 5 mN preload force in the compression mode. The compressive moduli were converted to shear moduli (G' and G'' at 1 Hz) using the relation $G = E/[2(1 + \nu)]$, where ν is the Poisson ratio assuming $\nu = 0.5$, which is a reasonable assumption for hydrogels.[42,43]

2.6. Characterization of Hydrogel High-Frequency Viscoelastic Moduli via Sensor Data and Fluid−Structure Interaction Models. While low-frequency G' and G'' (i.e., G' and G'' at 1 Hz) can be obtained from a dynamic mechanical analysis, G' and G'' at f can be obtained from cantilever fluid−structure interaction theory and

https://doi.org/10.1021/acsapm.2c00634
ACS Appl. Polym. Mater. 2022, 4, 5596−5607

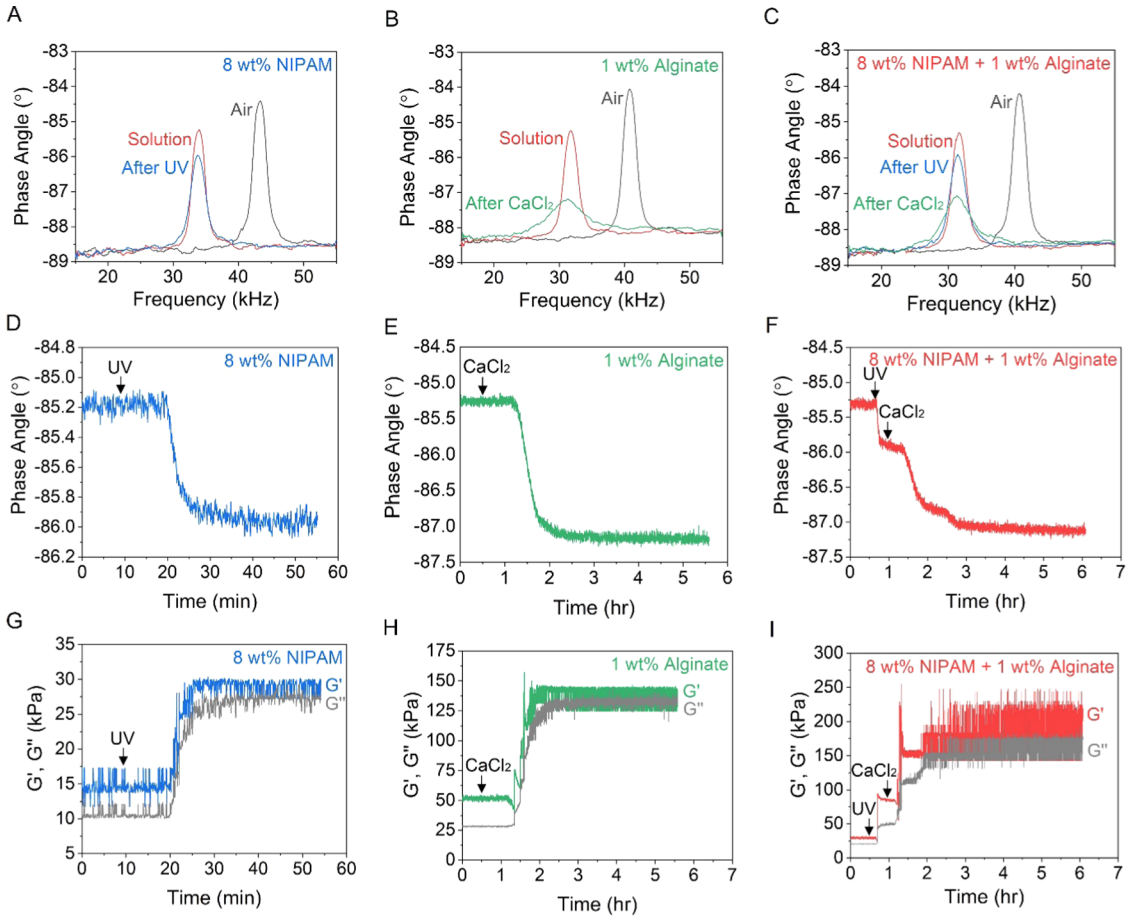

Figure 2. PEMC sensor impedance spectra (phase shift) in air, solution, and hydrogel for PNIPAM (A), alginate (B), and composite PNIPAM–alginate (C) precursor solutions and hydrogels. Real-time monitoring of PNIPAM, alginate, and composite PNIPAM–alginate hydrogel gelation via continuous tracking of phase angle at resonance (ϕ) (D–F) and associated real-time change in high-frequency shear moduli (G', G'') at the resonant frequency (f) (G–I).

experimentally measured f and quality factor (Q) response. A detailed description of the fluid–structure interaction model and underlying assumptions for piezoelectric milli-cantilever sensors can be found in our previous work.[35]

2.7. Characterization of Hydrogel Network Structure via Scanning Electron Microscopy. The network structures of the swollen hydrogels below and above the volume phase transition temperature (VPTT) of PNIPAM were characterized using variable-pressure scanning electron microscope systems (Hitachi SU-5000 and Hitachi SU-6600). Prior to mounting the membranes, each sample was first hydrated in deionized water for at least 24 h. To image the network structure above the VPTT, the hydrogels were heated to 55 °C in a water bath for 4 h before being flash-frozen using liquid nitrogen; samples below the VPTT were not heated but were subjected to the same flash-freezing procedure as those samples that were. All hydrogels (samples 5 × 15 × 20 mm^3) were then dried by lyophilization for 24 h at −105 °C; (FreeZone; Labconco). Prior to inserting samples into the SEM, the samples were attached by conductive adhesive tape to an aluminum specimen holder and sputter-coated with a thin layer of platinum (~3 nm; Anatech LTD Hummer 6.2).

3. RESULTS AND DISCUSSION

3.1. Real-Time Sensor-Based Monitoring of ICE Composite PNIPAM–Alginate Hydrogel Gelation. Schematics associated with the PEMC sensor design, measurement format, crosslinking steps, and network structure of ICE composite PNIPAM–alginate hydrogels are shown in Figure 1. As shown in Figure 1A,B, hydrogel viscoelastic property monitoring is performed by continuous monitoring of resonance in submerged piezoelectric milli-cantilever sensors. Sample (precursor solution) volumes of 250–1000 μL were used in this study. NIPAM monomer was first photocured to form a PNIPAM network. The alginate network was subsequently formed by chemical crosslinking with calcium chloride solution to create an ICE PNIPAM–alginate network (see Figure 1C). We note that other calcium-containing salts, which may exhibit different crosslinking rates and resultant hydrogel properties and characteristics (e.g., sample homogeneity), can also facilitate alginate crosslinking.[44] Here, we utilized calcium chloride based on its extensive use in additive manufacturing applications.[45] No phase separation was observed during reactions. The resultant composite PNIPAM–alginate hydrogels were transparent. We found that in the absence of temperature control (e.g., via the water bath) that maintains the temperature below LCST, hydrogels appeared opaque due to the heat released during polymerization.

Given that composite PNIPAM–alginate hydrogels are formed by interpenetrating networks of PNIPAM and alginate, PNIPAM and alginate hydrogels served as controls for the study. As shown in Figure 2A–C, PEMC enabled characterization of NIPAM, alginate, and composite PNIPAM–alginate hydrogel gelation, respectively, via phase angle response over

https://doi.org/10.1021/acsapm.2c00634
ACS Appl. Polym. Mater. 2022, 4, 5596–5607

the 15−55 kHz frequency range (f_{air} = 40.75 kHz). Submersion of the sensor in precursor solution caused a significant decrease of the ϕ, Q, and f based on a combination of fluid added mass and damping effects (f_{sol} = 31.7 kHz). Gelation of the precursor solution by photocuring or chemical crosslinking resulted in a significant change in ϕ (i.e., resonance amplitude), while only a minor shift in f was observed. This result is consistent with our previous study of sensor-based monitoring of alginate gelation.[35,36] Real-time monitoring of the composite PNIPAM−alginate hydrogel gelation process via continuous tracking of ϕ in comparison with control PNIPAM and alginate hydrogels is shown in Figure 2D−F. The f and Q responses are provided in Supporting Information Figure S2. The formation of the PNIPAM network caused a relatively smaller ϕ change than alginate network formation (19.2 ± 1.3 vs 52.7 ± 3.5%; n = 5; p = 0.05). As shown in Figure 2G−I, the real-time sensor data (f and Q, which is correlated with ϕ) facilitates real-time monitoring of the hydrogel viscoelastic property changes during the two-step reaction based on a fluid−structure interaction model of Mather et al.[35−37,41]

$$g_1 = \frac{\pi}{2}\frac{b_2 G''}{\omega} + \frac{\pi}{4\sqrt{2}}\sqrt{\rho}\, b[(b_1 - a_2)\sqrt{\sqrt{G'^2 + G''^2} + G'} + (a_2 + b_1)\sqrt{\sqrt{G'^2 + G''^2} - G'}] \quad (1)$$

$$g_2 = \frac{\pi}{4}a_1\rho b^2 + \frac{\pi}{2}b_2\frac{G'}{\omega^2} + \frac{\pi}{4\sqrt{2}}\frac{\sqrt{\rho}\, b}{\omega}[(b_1 + a_2)\sqrt{\sqrt{G'^2 + G''^2} + G'} + (a_2 - b_1)\sqrt{\sqrt{G'^2 + G''^2} - G'}] \quad (2)$$

$$g_1 = \frac{\pi}{4}\rho b^2\omega\left(\frac{\frac{(m_c + m_A)\omega}{Q} - c_i}{\rho b^2 L\omega\frac{\pi}{4}}\right) \quad (3)$$

$$g_2 = \frac{\pi}{4}\rho b^2\left(\frac{4\mu\left(\frac{\omega_o^2}{\omega^2} - 1\right)}{\pi b^2\rho}\right) \quad (4)$$

where L is the cantilever length, $\mu = \rho_c bt$ is the cantilever mass per unit length, ρ_c and t are the respective cantilever density and thickness, Q_0 and ω_o are the respective quality factor and resonant frequency in the absence of fluid damping (i.e., resonating in vacuum with only internal damping effects present), $m_c = \rho_c btL$ is the cantilever mass, $m_A = \rho\pi b^2 L\Gamma'/4$ is the added mass, Γ' is the real part of the hydrodynamic function, and $c_i = m_c\omega_o/Q_0$ is the internal damping coefficient. Due to the scale of the cantilevers (L = 4.1 mm,) the internal damping was not negligible and was subtracted from the measured value (as described in the term c_i in eq 3). In the calculation of c_i, ω_o and Q_0 were approximated as $\omega_o \sim 2\pi f_{n,air}$ and $Q_0 \sim Q_{n,air}$, which were reasonable assumptions as discussed in the following sections. The hydrodynamic function was approximated using the relation $\Gamma' = a_1 + a_2\,\delta/b$, where $\delta = [2\eta/(\rho\omega)]^{1/2}$ is the thickness of the thin viscous layer surrounding the cantilever in which the velocity has dropped by a factor of $1/e$ and η is the viscosity of the fluid. Given the significant change in resonance amplitude associated with gelation, this study focused on characterization of ICE hydrogel gelation based on real-time monitoring of ϕ, G', and G''. In Figure 2G−I, G' and G'' at f increased throughout the gelation process, similar to the trend of low-frequency viscoelastic moduli.[46]

Having established the measurement principle and format associated with PEMC sensor-based real-time monitoring of composite PNIPAM−alginate hydrogel viscoelastic properties, we next examined the effect of hydrogel composition on the sensor response and associated viscoelastic properties. A comparison of the change in resonance amplitude (i.e., peak height = $\phi - \phi_0$) associated with PNIPAM and alginate network formation during composite gelation is shown in Figure 3A using PNIPAM and alginate as negative controls

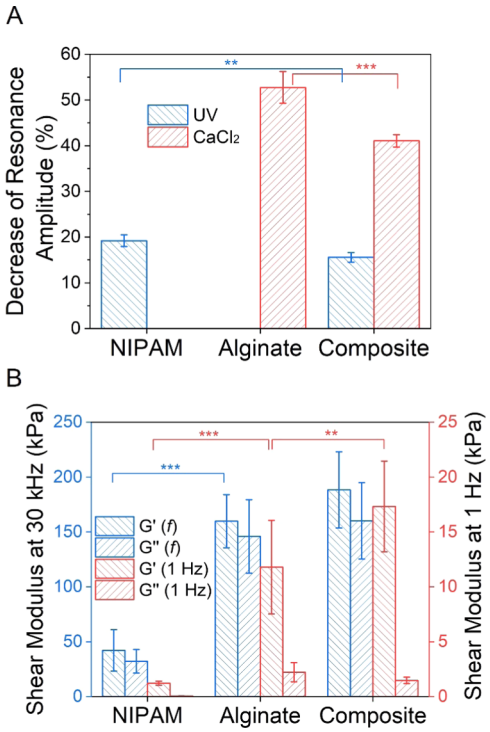

Figure 3. (A) Comparison of the resonance amplitude change (i.e., peak height change) at each step of the gelation process. (B) Comparison of shear moduli (G', G'') at the resonant frequency (f) obtained by sensing with G' and G'' at 1 Hz obtained by DMA, assuming Poisson ratio (ν) = 0.5 for PNIPAM, alginate, and composite PNIPAM−alginate hydrogels (NIPAM G'' data not visible on scale; ** and *** indicate $p < 0.01$ and $p < 0.001$, respectively).

(i.e., gelation in the absence of the other species). We found that both the change in resonance amplitude and viscoelastic properties caused by both PNIPAM and alginate network formation were lower in the composite PNIPAM−alginate hydrogel than in pure control hydrogels. For example, photocuring of NIPAM solution in the absence of alginate resulted in a 19.2 ± 1.3% decrease of the resonance amplitude, while photocuring of NIPAM solution that contained alginate, which we refer to as the composite hydrogel precursor solution, decreased to a lesser extent (15.55 ± 1.05%). Similarly, chemical crosslinking of alginate solution in the absence of PNIPAM caused the resonance amplitude to decrease by 52.7 ± 3.5%, while chemical crosslinking of the composite PNIPAM−alginate hydrogel caused a decrease of 41.1 ± 1.4%. This result suggests that the presence of the additional macromolecular component potentially affected the network structure relative to that achieved in hydrogels that

https://doi.org/10.1021/acsapm.2c00634
ACS Appl. Polym. Mater. 2022, 4, 5596−5607

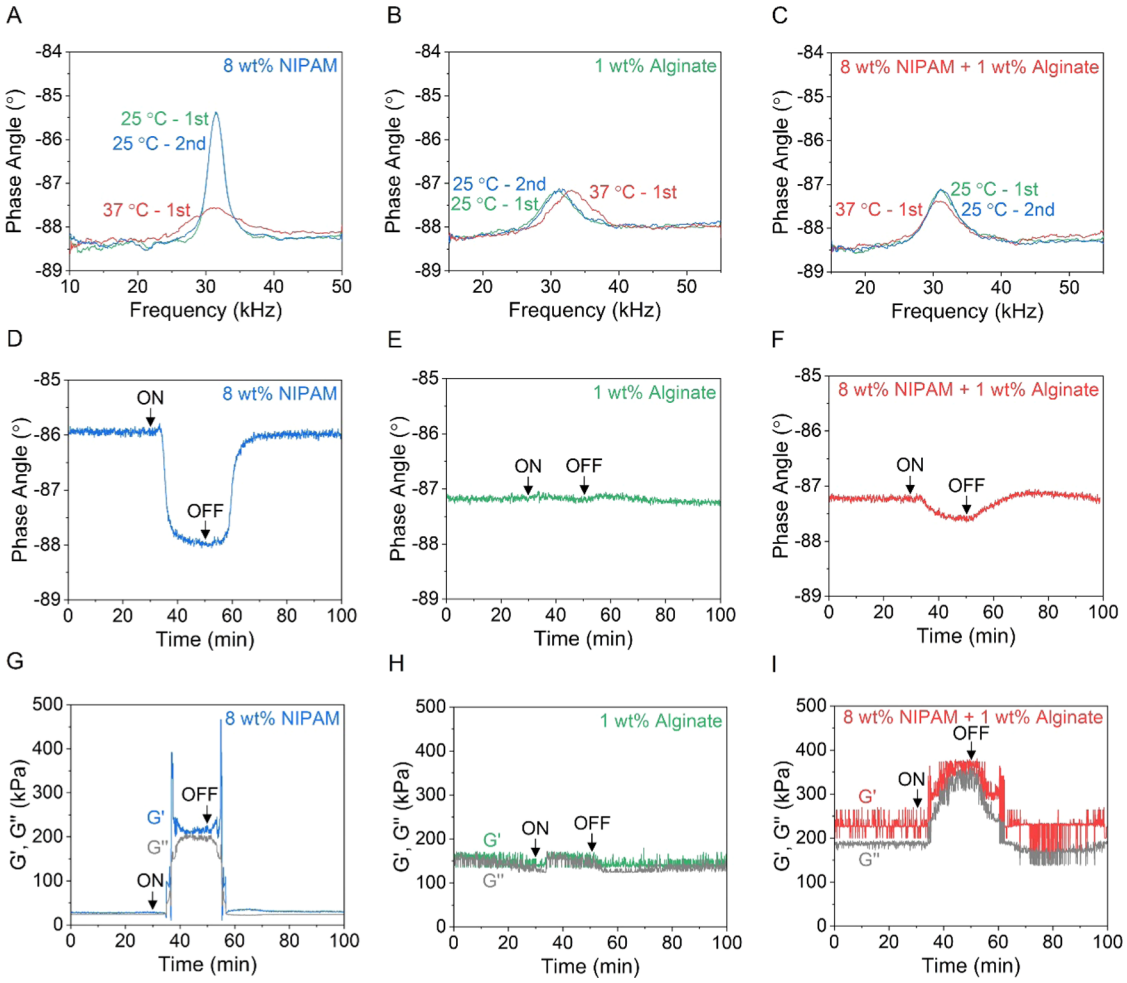

Figure 4. PEMC sensor impedance spectra (phase shift) in NIPAM (A), alginate (B), and NIPAM−alginate (C) hydrogels at T = 25 and 37 °C, and after one heating−cooling cycle. Real-time monitoring of phase angle (ϕ) (D−F) and shear moduli (G' and G'') at the resonant frequency (f) (G−I) throughout a heating−cooling cycle of PNIPAM, alginate, and composite PNIPAM−alginate composite hydrogel.

involve a single macromolecular component (e.g., pure PNIPAM and alginate hydrogels). This is a reasonable observation, given the remaining free volume within the network in the case of the composite systems, which can be occupied by an interpenetrating network. The total decrease in the resonance amplitude caused by composite PNIPAM−alginate hydrogel gelation (50.2 ± 1.3%) was comparable to that achieved by pure alginate hydrogels (52.7 ± 3.5%). A comparison of shifts in f and Q caused by gelation is provided in Supporting Information Figure S3.

In addition to the change (decrease) of resonance amplitude, real-time monitoring of ϕ also provided insight into dynamic processes, such as the reaction kinetics (e.g., photopolymerization reaction) and mass transfer processes (e.g., monomer or crosslinker diffusion) that drive the gelation process. A comparison of the data shown in Figure 2D−I shows that alginate gelation was slower in the presence of a crosslinked PNIPAM network compared to the absence of PNIPAM (i.e., for pure alginate hydrogels). This observation is consistent with the decreased diffusivity of Ca^{2+} ions through a polymer network relative to the solution. Thus, these results suggest that PEMC sensors provide a useful analytical platform for investigating the dynamic processes that drive hydrogel property response to external stimuli.

It is well established that G' scales as $\omega^{0.5}$ for many crosslinked polymers near the gel point, such as biomaterials.[47−49] In the gel phase, the increase in $G'(\omega)$ at high frequencies is because the bond lifetime is now longer than the typical motion due to thermal fluctuations; thus, the system shows the typical increase in elasticity, as the system cannot relax fast enough.[48] However, while this is a general scaling law for biomaterials, previous research has shown that G' may also exhibit power-law relations across the $1−10^4$ rad/s angular frequency range.[48] A comparison of G' and G'' at 1 Hz and f (~30 kHz) obtained by DMA and the PEMC sensor, respectively, among the different hydrogels, is shown in Figure 3B. The G' at f was larger than the G' at 1 Hz by greater than one order of magnitude among all hydrogels, ranging from a factor of ~10 to 30. These observations are not unreasonable when we consider the magnitude of f compared to the inverse of the surrounding material relaxation time, which is relatively slow.[50] The ratio of G' at f to G' at 1 Hz obtained by DMA and sensor data in this study agree reasonably with microrheology studies, which reported $G'(2\pi f = 30\ \text{kHz})/G'(2\pi f = 1\ \text{Hz})$ ranged from ~10 to 100 for water and DNA hydrogels across the 20−50 °C temperature range.[48] The G' obtained by sensor data were 42.1 ± 18.9, 159.8 ± 24.2, and 188.4 ± 34.7 kPa for PNIPAM, alginate, and composite PNIPAM−alginate hydrogels, respectively. The corresponding G'' were 32.2 ± 10.8,

https://doi.org/10.1021/acsapm.2c00634
ACS Appl. Polym. Mater. 2022, 4, 5596−5607

145.9 ± 33.5, and 160.2 ± 34.8 kPa for PNIPAM, alginate, and composite PNIPAM−alginate hydrogels, respectively. In comparison, the G' obtained by DMA were 1.2 ± 0.2, 11.8 ± 4.3, and 17.3 ± 4.1 kPa for PNIPAM, alginate, and composite PNIPAM−alginate hydrogels, respectively. The corresponding G'' were 0.06 ± 0.01, 2.2 ± 0.9, and 1.5 ± 0.3 kPa for PNIPAM, alginate, and composite PNIPAM−alginate hydrogels, respectively. Importantly, G' and G'' at f obtained by sensing are correlated with G' and G'' obtained by DMA for composite PNIPAM−alginate hydrogels. In addition to understanding the dependency of G' on f (i.e., ω), we next compared results obtained by DMA and PEMC by examining the effect of the frequency on δ and $|G^*|$. High-frequency rheology data obtained by MEMS-based techniques, such as QCM-based methods, have also been validated previously by comparison with low-frequency rheology data obtained by dynamic mechanical analysis.[51] In that study, the resonant frequency changes associated with the first three odd resonant modes were utilized to characterize the high-frequency viscoelastic properties. Validation of QCM data against DMA data was previously done by comparison of δ vs $|G^*|$ obtained under the same conditions. Here, we found that δ and $|G^*|$ at 1 Hz obtained by DMA for the alginate, PNIPAM, and alginate−PNIPAM hydrogels were 2.9, 10.6, and 5.0° and 1.2, 12.0, and 17.4 kPa, respectively; δ and $|G^*|$ at ∼30 kHz obtained by PEMC for the alginate, PNIPAM, and alginate−PNIPAM hydrogels were 37.4, 42.4, and 40.4° and 53.0, 216.4, and 247.3 kPa, respectively. Thus, δ obtained at high-frequency was relatively increased than that observed at low frequency by DMA for similar $|G^*|$ across the materials investigated. This result is consistent with previous QCM-based studies, which showed that the viscoelastic phase lag of the third mode of QCM near 15 MHz was relatively increased in polybutadiene and styrene−butadiene compared with that observed by DMA.[51] Differences in the change of δ between low- and high-frequency in this study and the aforementioned QCM-based study are attributed to differences in the range of the complex moduli investigated (kPa vs MPa−GPa, respectively) and mode type used for rheological characterization (second-order bending mode near 30 kHz vs third-order shear mode near 15 MHz, respectively). While PEMC and QCM provide a sensor-based characterization of high-frequency viscoelastic properties that are consistent with DMA, PEMC sensors exhibit several advantages, particularly associated with the sensor form factor. One significant challenge in the materials science and engineering is the ability to characterize small sample volumes. Similar to QCM, which exhibits a surface area ∼1 cm^2, PEMC sensors also facilitate characterization of droplets by deposition on the top face of the cantilever (∼1 mm^2). However, the millimeter-scale dipstick-based form factor offers unique advantages over planar centimeter-scale QCM geometry in terms of accessibility to small sample containers through vertical submersion. For example, PEMC sensors are 1 mm in width, which enables submersion in a variety of plastic- and culture-ware, including microcentrifuge tubes and 96-well plates, which are commonly utilized in materials science and additive manufacturing applications. Thus, we next examined if the dynamic response of composite hydrogel viscoelastic properties could be continuously monitored during material stimulation to further support their use in future process monitoring applications.

3.2. Real-Time Sensor-Based Monitoring of ICE Composite PNIPAM−Alginate Hydrogel Thermal Response.

At present, while image-based methods facilitate real-time monitoring of stimuli-responsive hydrogel and LBL-cured construct geometry change under various stimuli, few methods enable real-time monitoring of construct property response to stimuli, such as dynamic response of viscoelastic properties. Thus, we next characterized the real-time viscoelastic property response of composite PNIPAM−alginate hydrogel constructs to thermal stimulation. Sensor-embedded PNIPAM, alginate, and composite PNIPAM−alginate hydrogels were heated from room temperature (25 °C) to body temperature (37 °C) and then cooled to 25 °C. The range was selected based on the potential biomedical applications. Figure 4A−C shows the effect of temperature on the sensor resonance amplitude when surrounded by the various hydrogels. The continuous ϕ responses to the temperature cycling (i.e., raw sensor time-series data) are shown in Figure 4D−F. The f and Q responses are provided in Supporting Information Figure S4. The sensor responses exhibited profiles associated with the conductive heating and cooling processes used for temperature control. The PNIPAM, alginate, and composite PNIPAM−alginate hydrogels stabilized at 16.6 ± 3.6, 18.1 ± 1.7, and 16.9 ± 1.0 min following the temperature step change from 25 to 37 °C, respectively. The dynamic response of the composite PNIPAM−alginate viscoelastic properties vs the control hydrogel responses based on the real-time sensor data and a fluid−structure interaction model are shown in Figure 4G−I.[35,36] The effect of temperature change on the hydrogel viscoelastic properties was significantly higher in PNIPAM and composite PNIPAM−alginate hydrogels relative to alginate hydrogels. The viscoelastic property response of PNIPAM to temperature cycling also exhibited two maxima of G' at f during the heating and cooling phases (see Figure 4G). A similar trend in G' was also present for the composite PNIPAM−alginate hydrogel (see Figure 4I). We note that this trend was not observable in the alginate hydrogel response (Figure 4H), suggesting that it may be associated with the thermal response of the PNIPAM network in the pure and composite hydrogel systems.

As shown in Figure 5A, the extent of change in the percentage of peak amplitude (i.e., ϕ) was dependent on the hydrogel type. PNIPAM exhibited the most extensive relative thermal response based on ϕ change, which decreased by 67.3 ± 4.4% upon heating from 25 to 37 °C. The composite PNIPAM−alginate hydrogels exhibited the second largest response to the thermal stimuli, which caused a decrease of the resonance amplitude by 20.7 ± 2.7%. The alginate hydrogel exhibited the smallest response to thermal stimuli (2.4 ± 4.7% decrease of resonance amplitude). This trend agrees with previously reported temperature response data.[52,53] For example, Safakas et al. found the thermo-induced response of alginate-*g*-PNIPAM hydrogels shifts according to the content of NIPAM. It is also well established that PNIPAM hydrogels exhibit relatively large changes in shape and properties upon temperature change, which is not the case for alginate. Thus, the composite PNIPAM−alginate hydrogel exhibited dynamic viscoelastic property changes that were intermediate of the single-component hydrogels.

Figure 5B provides a comparison of the temperature dependence of the viscoelastic properties of PNIPAM, alginate, and composite PNIPAM−alginate hydrogels. The G' at 25 °C was 42.1 ± 18.9, 159.8 ± 24.2, and 201.6 ± 24.0 kPa for PNIPAM, alginate, and composite PNIPAM−alginate, respectively. The temperature increase to 37 °C caused a significant

https://doi.org/10.1021/acsapm.2c00634
ACS Appl. Polym. Mater. 2022, 4, 5596−5607

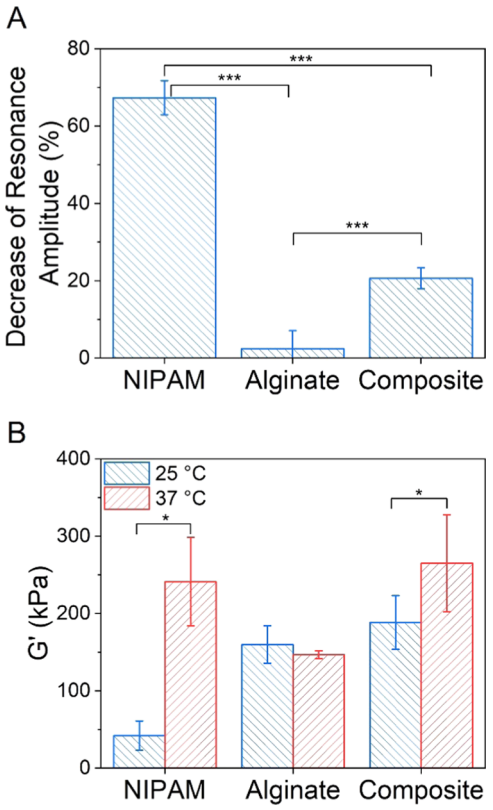

Figure 5. (A) Decrease of resonance amplitude (i.e., the difference between the phase angle ϕ at resonance and baseline value) after heating of PNIPAM, alginate, and composite PNIPAM−alginate hydrogels from 25 to 37 °C. (B) Storage modulus (G') at the resonant frequency (f) of PNIPAM, alginate, and composite PNIPAM−alginate hydrogels at 25 and 37 °C (* and *** indicate $p < 0.05$ and $p < 0.001$, respectively).

increase in G' of PNIPAM to 241.1 ± 57.2. In contrast, the temperature increase caused a small decrease in G' of alginate (146.7 ± 5.2 kPa). Similar to the PNIPAM hydrogel, the temperature increase from 25 to 37 °C was associated with an increase in G' of the composite PNIPAM−alginate hydrogel (290.5 ± 5.5 kPa). The sensor responses for PNIPAM hydrogels subjected to multiple temperature cycles are provided in Supporting Information Figure S5. Thus, the observed changes are consistent with the established knowledge of alginate and PNIPAM hydrogels, which further validated the use of PEMC sensors for real-time monitoring of stimuli-responsive hydrogel structure and properties.

As shown in Figure 6, the network structure of the composite PNIPAM−alginate hydrogels was significantly different below and above the VPTT (~32 °C), which supports the sensor data. PNIPAM hydrogels also exhibited significantly different network structures below and above the VPTT of PNIPAM (~32 °C; see Figure S6). Specifically, these SEM images capture the transition of the PNIPAM network structure from an expanded, open state with pores much larger than 100 μm to a tighter, collapsed network with pores on the order of 10 μm. The PNIPAM−alginate hydrogel constructs exhibited similar mesh sizes to neat PNIPAM hydrogels, which exhibited pore sizes on the order of hundreds of micrometers, below the VPTT of PNIPAM (see Figure S7).[54] Note that no pores smaller than those on the order of tens of micrometers were observed at higher magnification.

A similar transition in the network structure of the bulk-cured composite PNIPAM−alginate hydrogels was observed, where a tighter, more well-defined network structure with pore sizes on the order of tens of micrometers was observed for these materials once the samples were subjected to temperatures above that of the VPTT of PNIPAM (Figure 6A vs Figure 6C). The changes in the network structure captured by these SEM images help to elucidate the mechanism behind the enhancement in the storage moduli shown in Table 1, where,

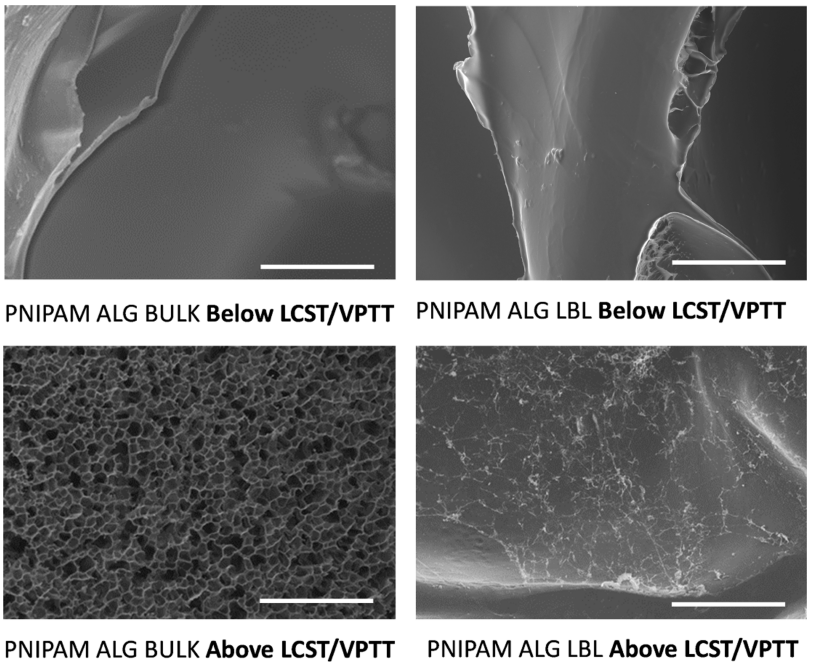

Figure 6. SEM of bulk- and layer-by-layer (LBL)-cured composite PNIPAM−alginate hydrogels below and above the VPTT of PNIPAM (scale bar = 100 μm).

https://doi.org/10.1021/acsapm.2c00634
ACS Appl. Polym. Mater. 2022, 4, 5596−5607

Table 1. Storage Modulus (G') at the Resonant Frequency ($f \sim 30$ kHz) of PNIPAM Hydrogels, Alginate Hydrogels, Bulk-Cured Composite PNIPAM−Alginate Hydrogels, and Layer-by-Layer (LBL)-Cured Composite PNIPAM−Alginate Constructs at 25 and 37 °C Calculated from Sensor Data and Cantilever Fluid−Structure Interaction Theory

hydrogel	G'-25 °C (kPa)	G'-37 °C (kPa)
PNIPAM	42.1 ± 18.9	241.1 ± 57.2
alginate	159.8 ± 24.2	146.7 ± 5.2
bulk-cured PNIPAM−alginate	201.6 ± 24.0	290.5 ± 54.5
LBL-cured PNIPAM−alginate	246.6 ± 67.7	408.2 ± 110.9

for example, the storage modulus of the bulk-cured composite PNIPAM−alginate hydrogel increased from 201.6 ± 24.0 to 290.54 ± 54.6 kPa, below and above the VPTT, respectively. However, the pore structure of these soft composites was more uniform, with smaller pore sizes than that observed for the neat PNIPAM samples (Figure 6C vs Figure S6B).

No well-defined network structure was observed on LBL-cured PNIPAM−alginate hydrogels above the VPTT, where only an apparent variation in the surface morphology was observed (Figure 6B vs Figure 6D). In fact, above the VPTT of PNIPAM, the soft composite appeared to phase-separate, creating a PNIPAM-rich phase with a web-like network structure and an alginate-rich phase with no apparent pores. The formation of this web-like structure by the PNIPAM provides physical insight into the mechanism of increased storage modulus and dynamic viscoelastic property response. Further, the fact that the PNIPAM phase-separated from the alginate may help to explain the larger increase in storage modulus below and above the VPTT for LBL-cured composite PNIPAM−alginate hydrogel (246.6 ± 67.6.0 to 408.2 ± 110.9 kPa) when compared to bulk-cured composite PNIPAM−alginate hydrogel (201.6 ± 24.0 to 290.54 ± 54.6 kPa), where the PNIPAM is prevented from phase-separating due to the fabrication method for these hydrogels.

3.3. Real-Time Monitoring of Composite PNIPAM−Alginate LBL Construct Gelation and Comparison of Bulk- vs LBL-Cured Construct Dynamic Viscoelastic Property Response. Stimuli-responsive hydrogels have great potential applications in additive manufacturing based on their ability to change shape and properties upon stimulation after fabrication. While a considerable number of studies have been reported on additively manufactured constructs, which utilize LBL deposition and curing processes, few studies and methods have characterized the real-time material assembly or dynamic response of bulk vs LBL-cured PNIPAM−alginate constructs. Thus, having monitored the real-time response of bulk-cured composite PNIPAM−alginate hydrogels to thermal stimuli, we next examined the assembly (gelation) and stimuli response of LBL-cured composite PNIPAM−alginate constructs to understand the potential impact of the fabrication (i.e., deposition and curing) approach (bulk- vs LBL-cured) on the network structure and dynamic viscoelastic response to thermal stimuli. An illustration of the LBL composite PNIPAM−alginate construct fabrication, which resembles an additive manufacturing process, is shown in Figure 7A. The average layer thickness was 0.6 mm based on the commonly used layer spacing in microextrusion 3D printing applications. Figure 7B highlights the effect of layer-curing of the impedance spectra of the PEMC sensor. Deposition of the polymer solution around the sensor caused a significant shift in both f and ϕ. Subsequent photocuring of each layer resulted in a continuous change of ϕ, as observed previously during the fabrication of bulk-cured composite PNIPAM−alginate hydrogels (see Figure 2). A significant decrease in ϕ was observed upon final chemical crosslinking of the four-layer LBL-photocured composite PNIPAM−alginate construct with $CaCl_2$. Figure 7C shows the real-time ϕ response during the LBL composite

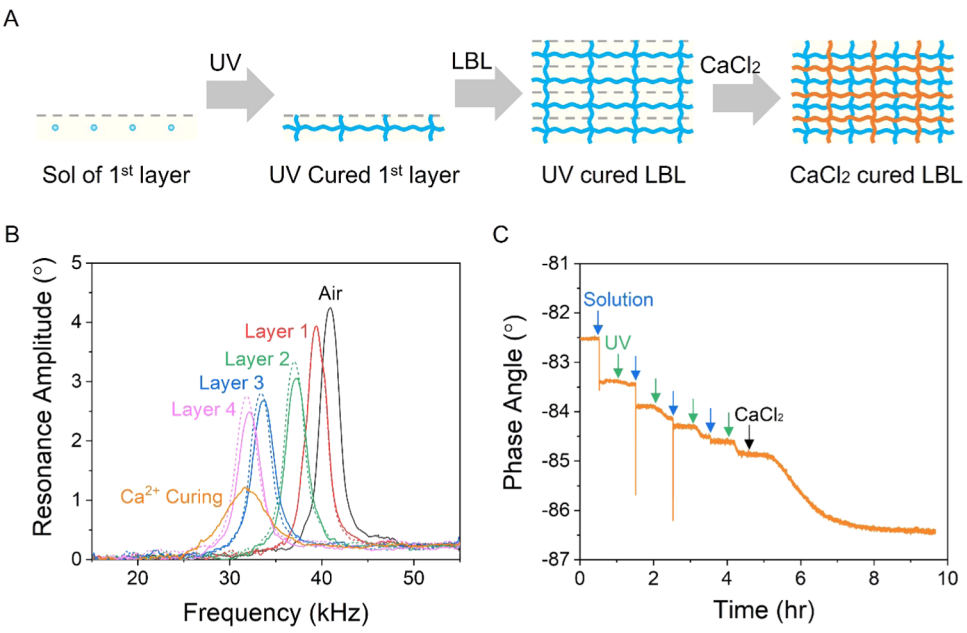

Figure 7. (A) Schematic illustrating the LBL fabrication process (deposition and curing) associated with the LBL-cured composite PNIPAM−alginate constructs. (B) Phase angle spectra from the cantilever sensor obtained at various times throughout the gelation process (dotted and solid lines indicate the sol and UV-cured gel state of each layer, respectively). (C) Real-time monitoring of LBL composite PNIPAM−alginate construct fabrication via continuous tracking of cantilever ϕ response.

https://doi.org/10.1021/acsapm.2c00634
ACS Appl. Polym. Mater. 2022, 4, 5596−5607

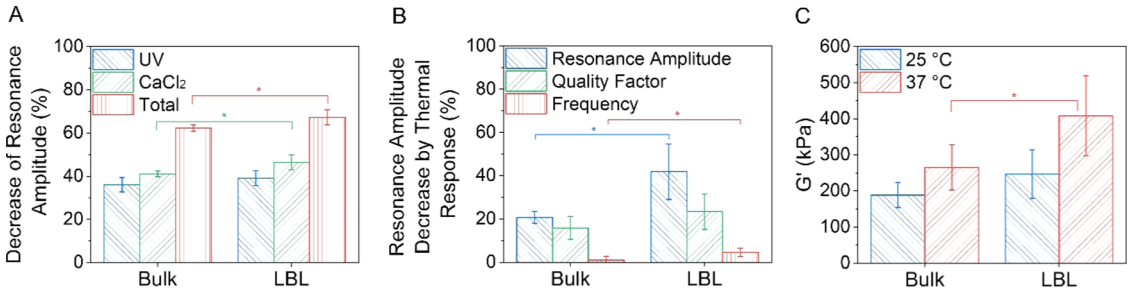

Figure 8. (A) Comparison of the resonance amplitude decrease caused by gelation for bulk and layer-by-layer (LBL) composite PNIPAM−alginate hydrogels (i.e., bulk- vs LBL-cured constructs). (B) Comparison of the percent decrease in resonance amplitude (peak height) caused by the thermal response of bulk and LBL composite PNIPAM−alginate hydrogels in terms of three sensor outputs from T = 25 and 37 °C. (C) Comparison of the storage modulus of bulk and LBL composite PNIPAM−alginate at T = 25 and 37 °C.

PNIPAM−alginate construct gelation process, which was composed of four subsequently photocured layers followed by a final chemical crosslinking of the LBL-cured construct. The real-time sensor response associated with the LBL processing is shown in Supporting Information Figure S8.

Having monitored the fabrication of LBL-cured composite PNIPAM−alginate constructs, we next compared their gelation and stimuli response with the previously examined bulk-cured samples. As shown in Figure 8A, the curing method had a significant effect on the change in ϕ (i.e., the expected change in G' associated with crosslinking). For bulk-cured composite PNIPAM−alginate hydrogels, the changes of ϕ caused by UV curing and $CaCl_2$ crosslinking were 36.0 ± 3.3 and 41.1 ± 1.4%, respectively. However, for LBL-cured composite PNIPAM−alginate constructs, the changes of ϕ associated with UV curing, $CaCl_2$ crosslinking, and the total change were 39.1 ± 3.5, 46.4 ± 3.5, and 67.3 ± 3.6%, respectively.

We then compared the real-time thermal response of bulk- and LBL-cured hydrogels via continuous monitoring of ϕ response. Figure 8B shows the percent change of ϕ upon heating the composite PNIPAM−alginate hydrogels from 25 to 37 °C, indicating 20.7 ± 2.7 and 41.9 ± 12.8% change for the bulk and LBL-cured composite hydrogels respectively (p = 0.022). Similarly, the bulk- and LBL-cured composite hydrogels exhibited significantly different percent changes in f from heating of 1.0 ± 1.8 and 4.6 ± 2.0% (p = 0.016). Next, we compared G' of bulk- and LBL-cured composite PNIPAM−alginate constructs at 25 and 37 °C (see Figure 8C). LBL-cured composite PNIPAM−alginate constructs exhibited a significantly larger G' change compared to bulk-cured constructs (p = 0.04). Thus, these studies suggest that the magnitude of dynamic viscoelastic property response of composite PNIPAM−alginate constructs is dependent on the processing method (e.g., material deposition-assembly and curing processes).

4. CONCLUSIONS

In this work, dynamic-mode piezoelectric milli-cantilever sensors were utilized to monitor the real-time gelation and thermal response of ionic−covalent entanglement composite PNIPAM−alginate hydrogel, a widely investigated stimuli-responsive hydrogel system. The dynamic response of composite PNIPAM−alginate viscoelastic properties during network formation and thermal stimulation were monitored in real time based on sensor data and established fluid−structure interaction models. Trends in shear moduli at the resonant frequency obtained by sensing correlated with compressive moduli data obtained by DMA. SEM captured the transition of the network structure of PNIPAM−alginate composite hydrogels below and above the VPTT of PNIPAM, which was quantitatively supported by changes in values of storage modulus with temperature. We also showed that the magnitude of dynamic viscoelastic property response in composite PNIPAM−alginate hydrogels is dependent on the fabrication method based on the comparison of bulk- and layer-by-layer constructs. In summary, piezoelectric milli-cantilever sensors are a useful experimental tool for characterization and real-time monitoring of hydrogel response to stimuli in practical low-volume measurement formats.

■ ASSOCIATED CONTENT

Supporting Information

The Supporting Information is available free of charge at https://pubs.acs.org/doi/10.1021/acsapm.2c00634.

Schematics of mold geometry, sensor resonant frequency, and quality factor data; sensor data associated with multiple temperature cycles; and SEM data of PNIPAM hydrogel samples (PDF)

■ AUTHOR INFORMATION

Corresponding Author

Blake N. Johnson − *Grado Department of Industrial and Systems Engineering, Macromolecules Innovation Institute, Department of Materials Science and Engineering, and Department of Chemical Engineering, Virginia Tech, Blacksburg, Virginia 24061, United States;* orcid.org/0000-0003-4668-2011; Phone: 540-231-0755; Email: bnj@vt.edu; Fax: 540-231-3322

Authors

Yang Liu − *Grado Department of Industrial and Systems Engineering and Macromolecules Innovation Institute, Virginia Tech, Blacksburg, Virginia 24061, United States*

Keturah Bethel − *Department of Chemical and Biomolecular Engineering, Clemson University, Clemson, South Carolina 29634, United States*

Manjot Singh − *Grado Department of Industrial and Systems Engineering, Virginia Tech, Blacksburg, Virginia 24061, United States*

Junru Zhang − *Grado Department of Industrial and Systems Engineering, Virginia Tech, Blacksburg, Virginia 24061, United States*

Rana Ashkar − *Macromolecules Innovation Institute and Department of Physics and Center for Soft Matter and*

https://doi.org/10.1021/acsapm.2c00634
ACS Appl. Polym. Mater. 2022, 4, 5596−5607

Biological Physics, Virginia Tech, Blacksburg, Virginia 24061, United States; orcid.org/0000-0003-4075-2330

Eric M. Davis − *Department of Chemical and Biomolecular Engineering, Clemson University, Clemson, South Carolina 29634, United States;* orcid.org/0000-0002-5633-5489

Complete contact information is available at: https://pubs.acs.org/10.1021/acsapm.2c00634

Notes

The authors declare no competing financial interest.

■ ACKNOWLEDGMENTS

This work was supported by GlycoMIP, a National Science Foundation Materials Innovation Platform funded through Cooperative Agreement DMR-1933525. The authors also acknowledge the support of the National Science Foundation under Grant Nos. CMMI-1739318 (B.N.J.), CMMI-2141008 (B.N.J.), and CBET-1403873 (E.M.D.). K.B. acknowledges the support of the Department of Education Graduate Assistance in Areas of National Need (GAANN) Fellowship Program (P200A180076). The authors also thank Missoury Lytle for assistance with characterization studies.

■ REFERENCES

(1) Lui, Y. S.; Sow, W. T.; Tan, L. P.; Wu, Y.; Lai, Y.; Li, H. 4D printing and stimuli-responsive materials in biomedical aspects. *Acta Biomater.* **2019**, *92*, 19−36.

(2) Kuang, X.; Roach, D. J.; Wu, J.; Hamel, C. M.; Ding, Z.; Wang, T.; Dunn, M. L.; Qi, H. J. Advances in 4D Printing: Materials and Applications. *Adv. Funct. Mater.* **2019**, *29*, No. 1805290.

(3) Zhang, L.; Yang, G.; Johnson, B. N.; Jia, X. Three-dimensional (3D) printed scaffold and material selection for bone repair. *Acta Biomater.* **2019**, *84*, 16−33.

(4) Döring, A.; Birnbaum, W.; Kuckling, D. Responsive hydrogels − structurally and dimensionally optimized smart frameworks for applications in catalysis, micro-system technology and material science. *Chem. Soc. Rev.* **2013**, *42*, 7391−7420.

(5) Hoffman, A. S. Stimuli-responsive polymers: Biomedical applications and challenges for clinical translation. *Adv. Drug Delivery Rev.* **2013**, *65*, 10−16.

(6) Dong, Y.; Wang, S.; Ke, Y.; Ding, L.; Zeng, X.; Magdassi, S.; Long, Y. 4D Printed Hydrogels: Fabrication, Materials, and Applications. *Adv. Mater. Technol.* **2020**, *5*, No. 2000034.

(7) Champeau, M.; Heinze, D. A.; Viana, T. N.; de Souza, E. R.; Chinellato, A. C.; Titotto, S. 4D Printing of Hydrogels: A Review. *Adv. Funct. Mater.* **2020**, *30*, No. 1910606.

(8) Zhou, W.; Qiao, Z.; Nazarzadeh Zare, E.; Huang, J.; Zheng, X.; Sun, X.; Shao, M.; Wang, H.; Wang, X.; Chen, D.; Zheng, J.; Fang, S.; Li, Y. M.; Zhang, X.; Yang, L.; Makvandi, P.; Wu, A. 4D-Printed Dynamic Materials in Biomedical Applications: Chemistry, Challenges, and Their Future Perspectives in the Clinical Sector. *J. Med. Chem.* **2020**, *63*, 8003−8024.

(9) Halperin, A.; Kröger, M.; Winnik, F. M. Poly(N-isopropylacrylamide) Phase Diagrams: Fifty Years of Research. *Angew. Chem., Int. Ed.* **2015**, *54*, 15342−15367.

(10) Bakarich, S. E.; Gorkin, R., III; Panhuis, M. I. H.; Spinks, G. M. 4D Printing with Mechanically Robust, Thermally Actuating Hydrogels. *Macromol. Rapid Commun.* **2015**, *36*, 1211−1217.

(11) Naficy, S.; Gately, R.; Gorkin, R., III; Xin, H.; Spinks, G. M. 4D Printing of Reversible Shape Morphing Hydrogel Structures. *Macromol. Mater. Eng.* **2017**, *302*, No. 1600212.

(12) Deng, Z.; Guo, Y.; Zhao, X.; Ma, P. X.; Guo, B. Multifunctional Stimuli-Responsive Hydrogels with Self-Healing, High Conductivity, and Rapid Recovery through Host-Guest Interactions. *Chem. Mater.* **2018**, *30*, 1729−1742.

(13) Han, D.; Lu, Z.; Chester, S. A.; Lee, H. Micro 3D Printing of a Temperature-Responsive Hydrogel Using Projection Micro-Stereolithography. *Sci. Rep.* **2018**, *8*, No. 1963.

(14) Sydney Gladman, A.; Matsumoto, E. A.; Nuzzo, R. G.; Mahadevan, L.; Lewis, J. A. Biomimetic 4D printing. *Nat. Mater.* **2016**, *15*, 413−418.

(15) Liu, J.; Erol, O.; Pantula, A.; Liu, W.; Jiang, Z.; Kobayashi, K.; Chatterjee, D.; Hibino, N.; Romer, L. H.; Kang, S. H.; Nguyen, T. D.; Gracias, D. H. Dual-Gel 4D Printing of Bioinspired Tubes. *ACS Appl. Mater. Interfaces* **2019**, *11*, 8492−8498.

(16) Liu, S.; Li, L. Ultrastretchable and Self-Healing Double-Network Hydrogel for 3D Printing and Strain Sensor. *ACS Appl. Mater. Interfaces* **2017**, *9*, 26429−26437.

(17) Zhou, Y.; Wan, C.; Yang, Y.; Yang, H.; Wang, S.; Dai, Z.; Ji, K.; Jiang, H.; Chen, X.; Long, Y. Highly Stretchable, Elastic, and Ionic Conductive Hydrogel for Artificial Soft Electronics. *Adv. Funct. Mater.* **2019**, *29*, No. 1806220.

(18) Hong, S.; Sycks, D.; Chan, H. F.; Lin, S.; Lopez, G. P.; Guilak, F.; Leong, K. W.; Zhao, X. 3D Printing of Highly Stretchable and Tough Hydrogels into Complex, Cellularized Structures. *Adv. Mater.* **2015**, *27*, 4035−4040.

(19) Rasool, A.; Ata, S.; Islam, A. Stimuli responsive biopolymer (chitosan) based blend hydrogels for wound healing application. *Carbohydr. Polym.* **2019**, *203*, 423−429.

(20) Bittner, S. M.; Pearce, H. A.; Hogan, K. J.; et al. Swelling Behaviors of 3D Printed Hydrogel and Hydrogel-Microcarrier Composite Scaffolds. *Tissue Eng., Part A* **2021**, *27*, 665−678.

(21) Jimenez-Vergara, A. C.; Lewis, J.; Hahn, M. S.; Munoz-Pinto, D. J. An improved correlation to predict molecular weight between crosslinks based on equilibrium degree of swelling of hydrogel networks. *J. Biomed. Mater. Res., Part B* **2018**, *106*, 1339−1348.

(22) Chang, C. Y.; Duan, B.; Cai, J.; Zhang, L. N. Superabsorbent hydrogels based on cellulose for smart swelling and controllable delivery. *Eur. Polym. J.* **2010**, *46*, 92−100.

(23) Shi, P.; Laude, A.; Yeong, W. Y. Investigation of cell viability and morphology in 3D bio-printed alginate constructs with tunable stiffness. *J. Biomed. Mater. Res., Part A* **2017**, *105*, 1009−1018.

(24) Hahn, L.; Maier, M.; Stahlhut, P.; Beudert, M.; Flegler, V.; Forster, S.; Altmann, A.; Töppke, F.; Fischer, K.; Seiffert, S.; Bottcher, B.; Luhmann, T.; Luxenhofer, R. Inverse Thermogelation of Aqueous Triblock Copolymer Solutions into Macroporous Shear-Thinning 3D Printable Inks. *ACS Appl. Mater. Interfaces* **2020**, *12*, 12445−12456.

(25) Nishi, K.; Hiroi, T.; Hashimoto, K.; Fujii, K.; Han, Y.-S.; Kim, T.-H.; Katsumoto, Y.; Shibayama, M. SANS and DLS Study of Tacticity Effects on Hydrophobicity and Phase Separation of Poly(N-isopropylacrylamide). *Macromolecules* **2013**, *46*, 6225−6232.

(26) Saunders, B. R. On the Structure of Poly(N-isopropylacrylamide) Microgel Particles. *Langmuir* **2004**, *20*, 3925−3932.

(27) Shibayama, M. Small-angle neutron scattering on polymer gels: phase behavior, inhomogeneities and deformation mechanisms. *Polym. J.* **2011**, *43*, 18−34.

(28) Pujals, S.; Feiner-Gracia, N.; Delcanale, P.; Voets, I.; Albertazzi, L. Super-resolution microscopy as a powerful tool to study complex synthetic materials. *Nat. Rev. Chem.* **2019**, *3*, 68−84.

(29) Kubota, R.; Torigoe, S.; Liu, S.; Hamachi, I. In Situ Real-time Confocal Imaging of a Self-assembling Peptide-grafted Polymer Showing pH-responsive Hydrogelation. *Chem. Lett.* **2020**, *49*, 1319−1323.

(30) Si, T. B.; Wang, Y. X.; Wei, W.; Lv, P.; Ma, G. H.; Su, Z. G. Effect of acrylic acid weight percentage on the pore size in poly(N-Isopropyl acrylamide-co-acrylic acid) microspheres. *React. Funct. Polym.* **2011**, *71*, 728−735.

(31) Mulakkal, M. C.; Trask, R. S.; Ting, V. P.; Seddon, A. M. Responsive cellulose-hydrogel composite ink for 4D printing. *Mater. Des.* **2018**, *160*, 108−118.

(32) Shin, S.; Hyun, J. Rheological properties of cellulose nanofiber hydrogel for high-fidelity 3D printing. *Carbohydr. Polym.* **2021**, *263*, No. 117976.

(33) Zhu, F.; Cheng, L.; Yin, J.; Wu, Z. L.; Qian, J.; Fu, J.; Zheng, Q. 3D Printing of Ultratough Polyion Complex Hydrogels. *ACS Appl. Mater. Interfaces* **2016**, *8*, 31304−31310.
(34) Karvinen, J.; Ihalainen, T. O.; Calejo, M. T.; Jönkkäri, I.; Kellomäki, M. Characterization of the microstructure of hydrazone crosslinked polysaccharide-based hydrogels through rheological and diffusion studies. *Mater. Sci. Eng. C* **2019**, *94*, 1056−1066.
(35) Haring, A. P.; Singh, M.; Koh, M.; Cesewski, E.; Dillard, D. A.; et al. Real-time characterization of hydrogel viscoelastic properties and sol-gel phase transitions using cantilever sensors. *J. Rheol.* **2020**, *64*, 837−850.
(36) Cesewski, E.; Singh, M.; Liu, Y.; Zhang, J.; Haring, A. P.; Johnson, B. N. Real-time monitoring of hydrogel rheological property changes and gelation processes using high-order modes of cantilever sensors. *J. Appl. Phys.* **2020**, *128*, No. 174502.
(37) Singh, M.; Zhang, J.; Bethel, K.; Liu, Y.; Davis, E. M.; Zeng, H.; Kong, Z.; Johnson, B. N. Closed-Loop Controlled Photopolymerization of Hydrogels. *ACS Appl. Mater. Interfaces* **2021**, *13*, 40365−40378.
(38) Chirra, H. D.; Hilt, J. Z. Nanoscale Characterization of the Equilibrium and Kinetic Response of Hydrogel Structures. *Langmuir* **2010**, *26*, 11249−11257.
(39) Matsui, S.; Nishizawa, Y.; Uchihashi, T.; Suzuki, D. Monitoring Thermoresponsive Morphological Changes in Individual Hydrogel Microspheres. *ACS Omega* **2018**, *3*, 10836−10842.
(40) Sharma, H.; Lakshmanan, R. S.; Johnson, B. N.; Mutharasan, R. Piezoelectric cantilever sensors with asymmetric anchor exhibit picogram sensitivity in liquids. *Sens. Actuators, B* **2011**, *153*, 64−70.
(41) Mather, M. L.; Rides, M.; Allen, C. R. G.; Tomlins, P. E. Liquid viscoelasticity probed by a mesoscale piezoelectric bimorph cantilever. *J. Rheol.* **2012**, *56*, 99−112.
(42) Chippada, U.; Yurke, B.; Langrana, N. A. Simultaneous determination of Young's modulus, shear modulus, and Poisson's ratio of soft hydrogels. *J. Mater. Res.* **2010**, *25*, 545−555.
(43) Gotou, R.; Shimizu, K. Slip Fracture and Shear Strength of Bentonite Gels. *Bull. Inst. Chem. Res., Kyoto Univ.* **1966**, *43*, 380−387.
(44) Kuo, C. K.; Ma, P. X. Ionically crosslinked alginate hydrogels as scaffolds for tissue engineering: Part 1. Structure, gelation rate and mechanical properties. *Biomaterials* **2001**, *22*, 511−521.
(45) Chimene, D.; Lennox, K. K.; Kaunas, R. R.; Gaharwar, A. K. Advanced Bioinks for 3D Printing: A Materials Science Perspective. *Ann. Biomed. Eng.* **2016**, *44*, 2090−2102.
(46) Bonino, C. A.; Samorezov, J. E.; Jeon, O.; Alsberg, E.; Khan, S. A. Real-time in siturheology of alginate hydrogel photocrosslinking. *Soft Matter* **2011**, *7*, 11510−11517.
(47) Murata, H. Rheology - Theory and Application to Biomaterials. In *Polymerization*; Gomes, A. D. S., Ed.; IntechOpen, 2012; Chapter 17.
(48) Xing, Z. Y.; Caciagli, A.; Cao, T. Y.; Stoev, I.; Zupkauskas, M.; O'Neill, T.; Wenzel, T.; Lamboll, R.; Liu, D. S.; Eiser, E. Microrheology of DNA hydrogels. *Proc. Natl. Acad. Sci. U.S.A.* **2018**, *115*, 8137−8142.
(49) Winter, H. H.; Chambon, F. Analysis of Linear Viscoelasticity of a Crosslinking Polymer at the Gel Point. *J. Rheol.* **1986**, *30*, 367−382.
(50) Janmey, P. A.; Georges, P. C.; Hvidt, S. Basic Rheology for Biologists. In *Methods in Cell Biology*; Academic Press, 2007; Vol. *83*, pp 1−27.
(51) Delgado, D. E.; Sturdy, L. F.; Burkhart, C. W.; Shull, K. R. Validation of quartz crystal rheometry in the megahertz frequency regime. *J. Polym. Sci., Part B: Polym. Phys.* **2019**, *57*, 1246−1254.
(52) Safakas, K.; Saravanou, S.-F.; Iatridi, Z.; Tsitsilianis, C. Alginate-g-PNIPAM-Based Thermo/Shear-Responsive Injectable Hydrogels: Tailoring the Rheological Properties by Adjusting the LCST of the Grafting Chains. *Int. J. Mol. Sci.* **2021**, *22*, 3824.
(53) Soledad Lencina, M. M.; Iatridi, Z.; Villar, M. A.; Tsitsilianis, C. Thermoresponsive hydrogels from alginate-based graft copolymers. *Eur. Polym. J.* **2014**, *61*, 33−44.
(54) Jian, Y.; Wu, B.; Yang, X.; Peng, Y.; Zhang, D.; Yang, Y.; Qiu, H.; Lu, H.; Zhang, J.; Chen, T. Stimuli-responsive hydrogel sponge for ultrafast responsive actuator. *Supramol. Mater.* **2022**, *1*, No. 100002.

https://doi.org/10.1021/acsapm.2c00634
ACS Appl. Polym. Mater. 2022, 4, 5596−5607